Theoretical Studies of Inorganic and Organometallic Reaction Mechanisms. 16. Oxidative Promotion of the Migratory Insertion of Carbon Monoxide in Cyclopentadienylmethyldicarbonyliron (II)

Zexing Cao,[†] Shuqiang Niu,[‡] and Michael B. Hall*

Department of Chemistry, Texas A&M University, College Station, Texas 77843

Received: December 23, 1999; In Final Form: May 9, 2000

Density functional methodology has been used to study the mechanistic details of the migratory insertion of CO into the transition metal−alkyl σ bond of the Fe cyclopentadienyl complexes $CpFe(CO)_2CH_3$ and $[CpFe(CO)_2CH_3]^+$ in the presence of phosphine, PH_3. Geometries, energies, and vibrational frequencies of reactants, molecular complexes, transition states, intermediates, and products are determined. Methyl migration with little PH_3 participation is the rate-determining step for both the neutral system and the cation system. Addition of PH_3 stabilizes the metastable intermediates $[CpFe(CO)(COCH_3)\text{- -}PH_3]^{0/+}$ and the products $[CpFe(CO)(COCH_3)(PH_3)]^{0/+}$. The calculated activation energies of the rate-determining steps are 17.8 and 7.5 kcal/mol for the neutral and cation reaction, respectively. The significant difference in these barriers is not due to the oxidatively promoted reaction utilizing a significantly different mechanism, but is interpreted in terms of methyl migration in the cation as having more radical character induced by the unpaired electron on Fe. For the reverse of the neutral migratory-insertion reaction, the overall activation energy is 24.3 kcal/mol. Thus, as is observed, the neutral reaction will be reversible only at higher temperatures. The overall exothermicities are −4.6 and −29.4 kcal/mol for the neutral and the cation reaction, respectively. The η^2-acyl intermediates $\{CpFe(CO)(COCH_3)\}^{0/+}$ are more stable by 6.1 and 11.1 kcal/mol than the η^2-methyl (agostic) intermediates, respectively. However, these η^2-acyl intermediates are not involved in the favored pathway of either reaction due to higher barriers for their formation. Natural bond orbital analyses for the molecular complexes $[CpFe(CO)_2(CH_3)\text{- -}PH_3]^{0/+}$ show a weak donor−acceptor interaction, where the phosphine behaves as acceptor in the neutral complex but as a donor in the cation.

Introduction

The complexes $CpFe(CO)_2R$ ($Cp = \eta^5\text{-}C_5H_5$) react with phosphine ligands (L) to form the acyl complexes $CpFe(CO)(COR)(L)$ (eq 1).

$$CpFe(CO)_2R + PR'_3 \rightarrow CpFe(CO)(COR)(PR'_3) \quad (1)$$

This reaction represents an example of migratory insertion of CO into a transition metal−alkyl bond, a reaction that is among the most thoroughly studied processes in organometallic chemistry because of its key role in various catalytic schemes for carbon monoxide activation.[1]

Initial kinetic studies on the mechanism of the migratory insertion have shown that the reaction is solvent dependent.[2a] At low concentrations the rate of reaction depends on ligand concentration [L] but a limiting rate is reached at high ligand concentrations.[2b] These results were explained in terms of a short-lived intermediate (Scheme 1)

SCHEME 1

$$(\eta^5\text{-}C_5H_5)Fe(CO)_2CH_3 \underset{k_{-1}}{\overset{k_1}{\rightleftharpoons}} \text{intermediate}$$

$$\text{intermediate} \underset{k_{-1}}{\overset{L,k_1}{\rightleftharpoons}} (\eta^5\text{-}C_5H_5)Fe(CO)(COCH_3)L$$

which may be solvated acyl iron compound $CpFe(CO)(COCH_3)(solvent)$.[2] An intermediate was also proposed by Green and Westlake.[3] Since they found no evidence of a solvated acyl iron compound, they suggested the formation of an intermediate like

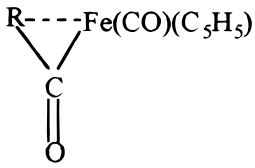

where the alkyl group R effectively takes up one coordination site in an agostic interaction. Wax and Bergman point out that solvent effects for this reaction are fairly small and differ from similar reactions of $CpMo(CO)_3CH_3$ in which large solvent effects were observed.[4]

Because of limitation of thermochemical techniques in elucidating the structure and reactivity of short-lived reactive intermediates in low steady-state concentrations,[1] definitive information about the intermediate of reaction 1 has not yet been obtained.

Laser flash photolysis of the acyl complex $(\eta^5\text{-}C_5H_5)Fe(CO)_2(COCH_3)$ leads to CO dissociation to generate the intermediate $(\eta^5\text{-}C_5H_5)Fe(CO)(COCH_3)$. The kinetic and spectroscopic properties of this reactive intermediate have been observed directly using time-resolved infrared technique (TRIR). In the absence of added substrates, the intermediate undergoes a rapid rearrangement to give the methyl complex $(\eta^5\text{-}C_5H_5)Fe(CO)_2CH_3$.[5]

In recent experimental studies of the phosphine-induced migratory-insertion reaction of the related indenyl complex (η^5-

* Corresponding author.
[†] On leave from Department of Chemistry, Xiamen University, Xiamen, Fujian 361005, China.
[‡] Present address: Pacific Northwest National Laboratory, Richland, WA.

10.1021/jp9944841 CCC: $19.00
Published on Web 07/14/2000

C_9H_7)Fe(CO)$_2$R (R = CH_3, $CH(CH_3)_2$), Monti and Bassetti proposed a mechanism involving (i) rapid formation of a molecular complex [(η^5-C_9H_7)Fe(CO)$_2$R- -phosphine] and (ii) rate-determining alkyl migration (Scheme 1).[6] These authors suggested that the molecular complex intermediate was formed by a weak interaction between phosphine and (C_9H_7)Fe(CO)$_2$R which does not perturb the molecular frame of the iron complex.[6] In this systematic kinetic investigation, no evidence of an η^3 intermediate, whose observation would support the hypothesis of ring slippage from an η^5- to η^3-bonding mode for the cyclopentadienyl and the indenyl ligands,[7,8] was found. A recent TRIR study of reactive intermediates in the photodecarbonylation of (η^5-C_5H_5)Fe(CO)$_2$(COCH$_3$) and (η^5-C_9H_7)Fe(CO)$_2$(COCH$_3$) shows that the photochemical properties of the indenyl and Cp compounds are quite similar and no significant difference in reactivity was observed.[5b] In contrast, a large difference of reactivity between the intermediates of the indenyl and Cp compounds is expected if a ring-slippage mechanism involving formation of an η^3 intermediate is the rate-determining process.[5c,5d]

For the migratory-insertion reaction of neutral (η^5-C_5H_5)Fe(CO)$_2$CH$_3$ induced by phosphines, preliminary kinetic investigations found activation energies of 18.2 ± 0.5 and 26.1 ± 0.6 kcal/mol, respectively, for PPhMe$_2$[3] and P(n-C_4H_9)$_3$.[2] For the indenyl complex (η^5-C_9H_7)Fe(CO)$_2$CH$_3$, the barrier for the rate-limited alkyl migration step is 18.8 ± 1 kcal/mol.[6]

The electrochemically induced oxidative promotion of the migratory-insertion reactions of these methyl iron complexes in the presence of donor ligands has also been investigated.[9] The experimental studies show that the oxidatively promoted migratory insertion is rapid in comparison to the neutral 18-electron parent complexes. In their investigation of the oxidative promotion of CO insertion in CpFe(CO)(PPh$_3$)CH$_3^+$, Therien and Trogler proposed that a key step was nucleophilic attack at the 17-electron metal center which results in formation of a 19-electron intermediate (Scheme 2, Nu = substituted pyridine).[9b]

SCHEME 2

$$\underset{18e}{CpFe(CO)(PPh_3)CH_3} \underset{+e^-}{\overset{-e^-}{\rightleftharpoons}} \underset{17e}{CpFe(CO)(PPh_3)CH_3^+}$$

$$\underset{17e}{CpFe(CO)(PPh_3)CH_3} + Nu \underset{k_{-1}}{\overset{k_1}{\rightleftharpoons}} \underset{19e}{CpFe(CO)(PPh^3)(Nu)CH_3^+}$$

$$\underset{19e}{CpFe(CO)(PPh_3)(Nu)CH_3^+} \underset{k_{-2}}{\overset{k_2}{\rightleftharpoons}} \underset{17e}{CpFe(Nu)(PPh_3)(COCH_3)^+}$$

In a more recent study of asymmetric migratory-insertion reactions of the chiral iron complex (BpDMCp)Fe(CO)$_2$CH$_3$ (BpDMCp = binaphthyldiyldimethylene-annulated cyclopentadienyl), Colletti and Halterman found that preparative-scale oxidatively promoted migratory-insertion reactions occur rapidly and that the 17-electron [(BpDMCp)Fe(CO)$_2$CH$_3$]$^+$ diastereomer with or without the addition of PPh$_3$ is configurationally stable.[9a]

Although many studies have been directed at these migration−insertion reactions, the mechanistic details, structures of the intermediates, effect of added phosphine, existence of molecular complexes, and nature of the oxidative acceleration are imprecisely understood. Previous theoretical studies have aided our general understanding of similar reactions. In particular, detailed theoretical studies on the migratory-insertion reactions of CO and NO into transition metal−carbon bonds of Mn(CO)$_5$CH$_3$ and CpCo(NO)CH$_3$, respectively, have been carried out at various levels.[10−18] These calculations come to the conclusion that these reactions take place via methyl migration to a bound CO or NO followed by coordination of the additional donor ligand.

Here, we report a full theoretical treatment of the migratory-insertion reaction of neutral (η^5-C_5H_5)Fe(CO)$_2$CH$_3$ (**2**) and its cation (**2**+) in the presence of PH$_3$ (**1**). The geometries and energies of reactants, molecular complexes, intermediates, transition states, and products have been determined by density functional theory (DFT). Vibrational properties of the acyl and CO along the migratory-insertion reaction path, bonding in the molecular complex, and differences between the reactivity of the neutral and the cation system are discussed.

Computational Details

Becke's three-parameter hybrid exchange functional[19] has been combined with Lee−Yang−Parr's nonlocal correlation functional[20] (B3LYP) and the default fine integration grid implemented in the Gaussian 94 program[21] has been used in all DFT calculations. At the DFT level, natural population analyses (NPA) and natural bond orbital (NBO) analyses on relevant states have been performed.[22]

An effective core potential (ECP) for the iron has been employed in all DFT calculations. In the ECP the 3s and 3p orbitals were considered explicitly along with the 3d, 4s, and 4p valence orbitals. As a modification of the double-ξ ECP basis set of Hay and Wadt,[23] the 4p orbital of Fe was represented by a valence optimized function from Couty and Hall.[24] For atoms C, O, and P, the all-electron 6-31G basis sets[25−29] have been used. This basis set is designated as BS1. For the energy calculations and geometry optimization of several states important in the rate-determining step, these basis sets have been augmented by adding an f-type polarization function with a exponent of 2.462[30a] for Fe and d-type polarization functions for atoms C, O, and P (the 6-31G* basis sets). The augmented basis set is denoted as BS2. At the B3LYP/BS1 level, the association energy of PH$_3$ with the CpFe(CO)$_2$(CH$_3$) complex has been corrected for the basis set superposition error (BSSE)[30b] and the zero-point energy (ZPE).

Results

Neutral Systems. *Reaction Path.* The stationary points on the potential energy surfaces at the DFT level for the lowest energy paths in the neutral process are displayed in Figure 1. As shown in Figure 1, the formation of the molecular complex **3** from **1** + **2** is exothermic by −1.78 kcal/mol. After correction for the basis set superposition error (BSSE), formation of the molecular complex **3** is still exothermic by −1.19 kcal/mol. The binding energy for the molecular complex **3** is reduced to 0.74 kcal/mol after addition of zero-point vibrational energies. From this weakly bound complex the reaction proceeds via the first transition state **4** with a barrier of 17.3 kcal/mol to an agostic intermediate **5**. The methyl migration process from **3** to **5** is the rate-determining step for the overall reaction. Intermediate **5** is higher in energy than the molecular complex **3** by 16.6 kcal/mol, and easily returns to the molecular complex **3** through an intramolecular rearrangement with a very low barrier. The instability of this intermediate will make its detection difficult.

In intermediate **5** the phosphine is still only weakly bound to the Fe complex. As the phosphine approaches closer to the Fe, the agostic interaction weakens as the system reaches the second transition state, **6**, which is 4.8 kcal/mol above the agostic intermediate **5**. The reaction then proceeds to the products. First,

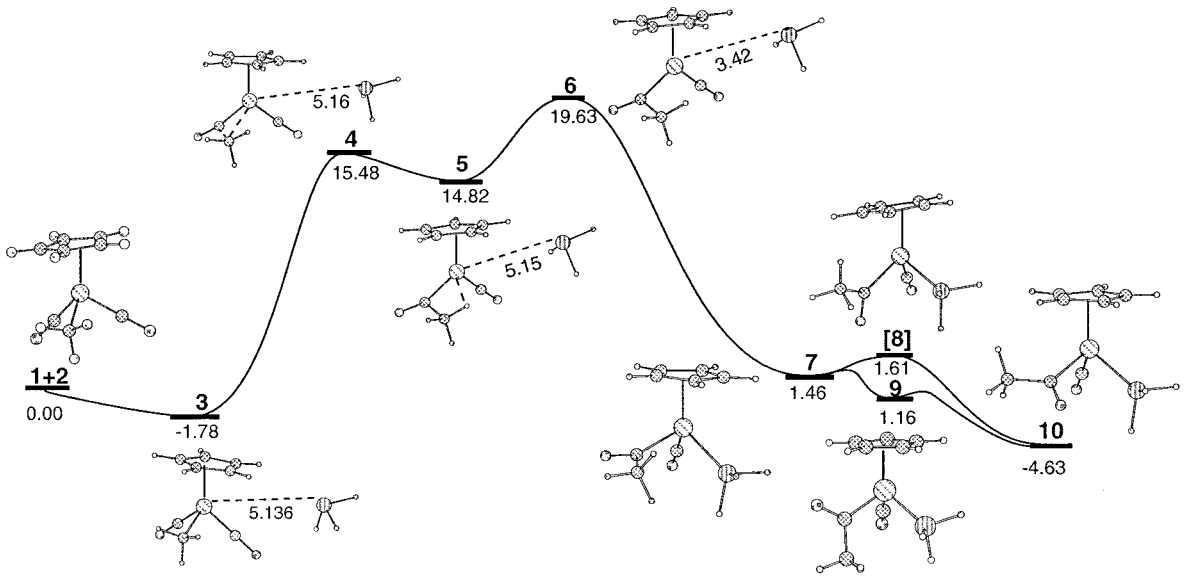

Figure 1. Profiles of the potential energy surfaces for the favored mechanism in the neutral reaction.

the product in conformation **7** is formed, then the most stable conformation **10** is formed by a rotation of the MeC(O)−Fe either counterclockwise through **8** (an approximate transition state) or clockwise through **9**. Overall the product is 4.6 kcal/mol more stable than the reactants.

Energetics. Using the larger basis set (BS2), we reoptimized the geometries of the molecular complex **3** and the transition state **4**, which are responsible for the rate-determining step, and no notable disparity in geometry was observed compared with results at level of BS1. Full geometry optimizations with BS2 gave the rate-determining activation energy of 17.8 kcal/mol. The activation energy obtained by single-point calculations with BS2 at the BS1 optimized geometries is 17.7 kcal/mol, while that for BS1 was 17.3 kcal/mol. These calculated activation energies are in reasonably good agreement with the experimental value for the smaller phosphine of 18.2 ± 0.5 kcal/mol.[3] Since there is almost no barrier for the intramolecular rotation from **7** to **10**, the overall barrier for the reverse reaction from the product **10** to the active intermediate **5** is about 24.3 kcal/mol at the BS1 level. Presumably, the neutral migration reaction would only be reversible at higher temperatures as others have concluded experimentally.[9a]

Geometries. Figure 2 displays the fully optimized geometries of the reactants PH_3 (**1**) and $CpFe(CO)_2CH_3$ (**2**), molecular complexes, intermediates, transition states, and products for the neutral systems. Comparison of the available experimental values with calculated values in Table 1 shows that the B3LYP method even in the double-ξ basis set gives a reliable prediction of the equilibrium geometries.

From Figure 2, it can be noted that the distances between Fe and the centroid of the Cp ring at first contracts from 1.82 Å in **2** to 1.79 Å in **5** then lengthens again to 1.84 Å in the product **10**. In a corresponding way the Fe−C bond length for the inactive CO first lengthens and then contracts, while C−O length increases gradually from 1.173 to 1.180 Å along the reaction path. The bond length of the active CO lengthens significantly from 1.173 in the reactant **2** to 1.206 Å in the transition state **4**, and finally to 1.251 Å in the product **10**. The bond length change of the active CO displays the expected conversion from a triple to a double bond. Because of the low stability of intermediate **5**, transition state **4** displays bond lengths characteristic of a late transition state with a short H_3C- -CO and a considerably lengthened C−O.

The weak bonding of the phosphine in the molecular complex **3** results in few geometric changes compared to **2**. This is in agreement with recent experiments which showed that the phosphine does not perturb the molecular frame of the alkyl Fe complex and the indenyl ligand remains in η^5 coordination.[6] In spite of starting geometries with several other positions for the PH_3, all optimized to a structure like **3**, where PH_3 is between the ring and the carbonyl group. The orientation of the PH_3 always shows an alignment along the P−H direction. The P−H distances in the molecular complex **3** are asymmetric with two slightly shorter in comparison with that of an isolated PH_3 (1.450 Å) and the third nearly identical to that in a free ligand.

In the intermediates **5**, the distance of the agostic Fe- -HCH_2 is 2.030 Å. The agostic interaction results in a lengthening of this C−H bond to 1.115 Å compared with other C−H bond lengths of 1.092 Å. Note that the Fe−C−C angle is reduced from ∼120° to 84° by the agostic interaction.

Cation Systems. *Reaction Path.* The stationary points on the potential energy surface for the oxidatively promoted process are displayed in Figure 3. These calculations show that the oxidatively promoted reaction includes (i) the rate-determining methyl migration from **3**+ over transition state **4**+ to **5**+, (ii) followed by rapid association of PH_3 to produce **7**+ and (iii) an intramolecular rotation of the MeC(O)−Fe either clockwise through **8**+ or counterclockwise through **9**+ to form the final product **10**+. In comparison with the separated reactants **1** and **2**+, the molecular complex **3**+ is more stable by 5.8 kcal/mol. The barrier of the rate-determining step is only 7.6 kcal/mol. The metastable intermediate **5**+ for the oxidatively promoted reaction is more stable than the transition state **4**+ by 1.5 kcal/mol. From the initial product **7**+ the lower barrier corresponding to intramolecular rotation is 3.8 kcal/mol. The final product **10**+ is more stable than the molecular complex **3**+ by −29.4 kcal/mol. DFT calculations with the larger basis set, BS2, predicted a similar activation energy (7.5 kcal/mol). Therefore, the overall cation reaction is predicted to be rapid as observed exprimentally.[9a]

Geometries. DFT-optimized geometries of relevant reactants, intermediates, transition states, and the product in the oxidatively promoted reaction are shown in Figure 4. The separations between Fe and the centroids of the Cp ring vary from 1.818 to 1.880 Å. The bond length of the inactive CO increases by 0.01 Å from the reactant **2**+ to the product **10**+, while that of the

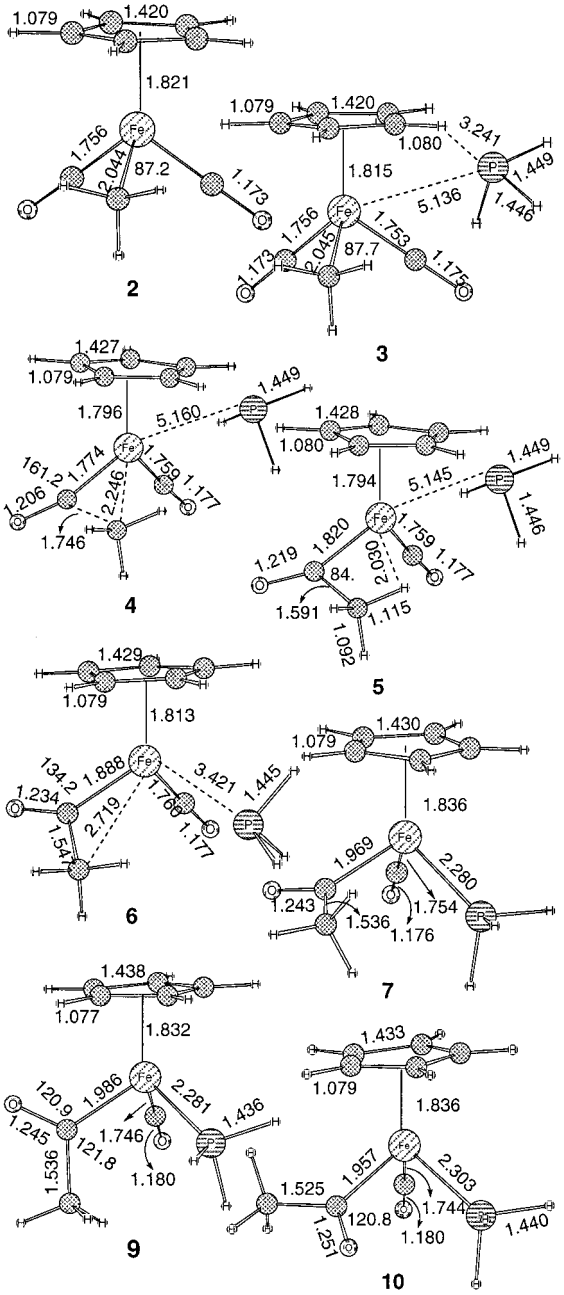

Figure 2. B3LYP-optimized geometries of the neutral reactant **2**, the molecular complex **3**, transition states **4** and **6**, intermediates **5**, **7**, and **9**, and the final product **10** (only selected C−C and C−H bond lengths are given for the Cp ring).

reactive CO increases from 1.153 to 1.230 Å, again revealing the conversion of the CO bond from a triple to a double bond. In the molecular complex **3**+, the orientation of PH_3 nearly shows alignment along the Cp plane. In the agostic intermediate **5**+, the Fe−HCH_2 distance is 2.100 Å, 0.07 Å longer than that in **5**.

Discussion

Energetic Differences. In addition to being kinetically favorable compared to the neutral process, the oxidatively promoted reaction is much more exothermic. The origin of this significant difference in the reaction energy can be understood by application of a generalized Born−Fajans−Haber cycle to these two processes, Scheme 3, where ΔE_1, ΔE_2, IP_1, and IP_2 represent, respectively, the reaction energies of the neutral and cation processes, and ionization potentials of the neutral reactant and the neutral product (in kcal/mol). This cycle reveals that a much lower ionization potential of the product **10** compared to the reactant **2**, is the reason the cation process is so exothermic.

TABLE 1: Comparison of Selected Geometric Parameters of the Reactant and the Product[a]

species	calcd	expt[b]
$CpFe(CO)_2CH_3$		
Fe−CO	1.756	1.75
Fe−CH_3	2.044	1.99
OC−Fe−CH_3	87.2	86.
$CpFe(CO)(COCH_3)$		
Fe−CO	1.744	1.738(2)
Fe−$COCH_3$	1.957	1.956(3)
Fe−PR_3	2.303	2.214(1)
R_3P−Fe−$COCH_3$	88.0	89.5(1)

[a] Bond lengths in Å and angles in degrees. [b] Experimental values for the $CpFe(CO)_2CH_3$ and $CpFe(CO)(COCH_3)$ analogues are from $[CpFe(CO)_2C_2H_2]_2$32 and $(C_9H_7)Fe(CO)(COCHMe_2)(PPh_3)$,[33] respectively.

NBO analyses indicate the total antibonding occupancy in the reactant **2** is 2.67, while that of the $CpFe(CO)(COCH_3)$ fragment in the product **10** is 2.90. Therefore, the $CpFe(CO)(COCH_3)$ is a richer electron system in the product **10** compared to the reactant **2**. From Figure 5a, which displays the net charge variations for different subunits along the reaction path obtained by NPA,[22] one can note that 0.33 electrons contributed by PH_3 are ultimately reflected in an increase of antibonding occupancy by 0.23 in product **10**. These excess electrons will result in outer orbitals rising in energy. Figure 6 shows variations of these orbital energy levels. Therefore, the product **10** loses an electron more easily than the reactant **2**. Basically, PH_3 is a better donor and poorer acceptor than CO.

Geometrical Differences. Most bonds to Fe in the cation system except Fe−CH_3 are generally longer than those in corresponding neutral systems. These geometrical differences can be attributed to distinct bonding features between the cation and neutral systems. For example, when the neutral reactant **2** loses an electron, which leads to the cation reactant **2**+, the highest occupied molecular orbital (HOMO) in **2**, which contributes the bonding between the ring and Fe center, converts to a singly occupied HOMO (SOMO), behaving as a lone electron on Fe. This change weakens the back-donating interaction between the Fe center and all the other π acceptor ligands. Therefore, the distances between Fe and the centroids of the ring, and Fe−CO and Fe−$COCH_3$ bond lengths in the cation system are significantly longer than those in the neutral system, while the pure σ covalent bond to CH_3 shortens.

Mechanistic Differences. Unlike the neutral reaction, there is no barrier for phosphine to displace the agostic bond in the cation case. This difference can be attributed to the difference in the agostic interaction between the intermediates **5** and **5**+. From the geometries displayed in Figures 2 and 4, it may be seen that the Fe−H separation in **5** is slightly shorter than that in **5**+, while the C−C bond length of C(O)−CH_3 in **5** is longer than that in **5**+. These results suggest that the neutral agostic interaction should be stronger in **5** than that in the cation **5**+. The phosphine association, which must break the agostic interaction, has a barrier of 4.8 kcal/mol for the reaction of PH_3 with **5** to yield **7**. Because of a weaker agostic interaction, the barrier between **5**+ and **7**+ is negligible. The difference between **5** and **5**+ in their agostic bonds is due, in part, to the weaker back-bonding ability of Fe^{3+}. Additional factors contribute to this difference between the neutral and cation system. First, the cation is a stronger electrophilic acceptor with respect to the

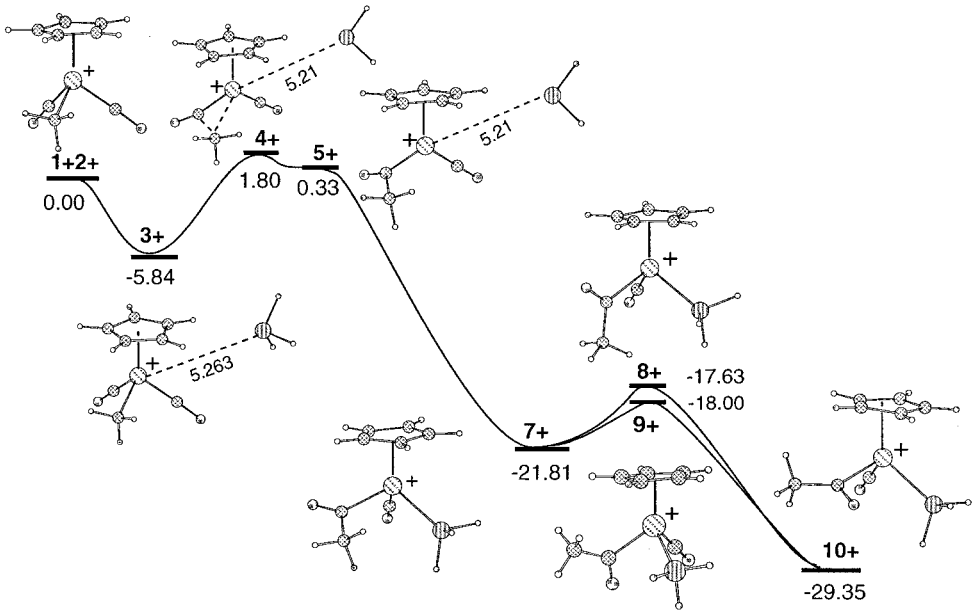

Figure 3. Profiles of the potential energy surfaces for the favored mechanism in the cation reaction.

phosphine, and second, the overall reaction is much more exothermic for the cation. The intramolecular rotation of the stable intermediate **7**+ leading to the product **10**+ must overcome a barrier of 3.81 kcal/mol, while for the neutral intermediate **7** no significant barrier was found.

Figure 7, a and b, displays the singly occupied molecular orbital (SOMO) in the cation reactant **2**+ and the highest occupied molecular orbital (HOMO) in the neutral reactant **2**. The significant difference between the rate-determining steps for these two processes can be understood by analyzing the effect of the SOMO of **2**+ on the reactivity. From Figure 7a, note that the SOMO is essentially composed of an Fe d orbital, which has a maxima in the path of the methyl migration. Furthermore, the SOMO is close in energy to the next MO, corresponding to the Fe−CH_3 bond. From an orbital point of view, the SOMO can mediate the Fe−CH_3 bond breaking and the OC−CH_3 bond making during the methyl migration of the cation reaction and promote the reaction.

Net charge variations along the reaction path for the neutral reaction, displayed in Figure 5a, show that the charge at the Fe center in the reactant **2** and the product **10** has no notable difference. The Fe center plays an agent's role in the charge transfer process from PH_3 to spectator ligands in the Fe complex. Interestingly, charge changes in Figure 5a show that the electron densities on the Fe and CH_3 decrease synchronously from the reactant **3** to the migration transition state **4**, while the electron density on spectator CO ligand significantly increases. These features of the electron density suggest that the Fe−CH_3 σ-bonding pair transfers to the CO π*, and makes a new quasi-bond C(O)−CH_3 in the transition state **4**. Thus, the methyl CH_3 will hold a lone pair of electrons as it migrates, migrating as :CH_3^-. However, for the cation system Figure 5b shows that the changes in charge for Fe and CH_3 are asynchronous from the molecular complex **3**+ to the transition state **4**+, where the electron density on the methyl CH_3 significantly decreases, while the electron density of Fe only slightly increases. The Fe−CH_3 bond electron density mainly transfers to the inactive CO ligand. This trend implies that the CH_3 is maintaining more radical character, namely ·CH_3, during the migration in the cation system. From **5** to **7** the neutral system's COs and Cp remove charge from Fe until the TS at **6**, when the PH_3 begins to become a strong donor. In the cation system there is hardly any barrier so PH_3 donation begins at **5**. Orbital analyses, as opposed to NBO analyses, of similar methyl migrations provide a somewhat different view of the details of the electron transfer process.[18] Perhaps even more important than the these details is the much larger exothermicity of the cation reaction, which alone can explain the lower barrier.

Within the restricted open-shell DFT formalism, we compared the singly occupied MOs of **3**+ and **5**+. The SOMO of **3**+ is the same as that of **2**+ depicted in Figure 7a, while the SOMO of **5**+ (Figure 7c) is mainly derived from the MO which accounts for the Fe−CH_3 bond in **3**+ (Figure 7d). This change in character of the SOMO during the migration implies that the methyl migration proceeds by polarizing the Fe−CH_3 bond to form a ·CH_3 quasi-radical then by coupling the ·CH_3 radical with the unpaired electron of the SOMO (Figure 7a) and finally by forming the C(O)−CH_3 bond. Combining the net charge and the MO analyses, one can conclude that the oxidatively promoted migration is a ·CH_3 quasi-radical transfer process, while a :CH_3^- ion transfer process is responsible for the neutral migratory-insertion.

Ring Slippage. The possibility of a ring-slippage mechanism has also been investigated. A five-coordinated Fe(II) intermediate, (η^2-Cp)Fe$(CO)_2CH_3PH_3$, corresponding to ring-slippage was completely optimized and is higher in energy than the molecular complex **3** by 28.4 kcal/mol. Thus, the ring-slippage mechanism would require greater activation energy then the mechanism in Figure 1. Attempts to find a ring-slipped intermediate for the cation failed; η^2 geometries and other initial five-coordinate Fe(II) complexes decay into the molecular complex **3**+ upon optimization. Therefore, the calculated results seem to rule out ring slippage as part of the mechanism of the migratory insertion in the cyclopentadienyl Fe complex. Recent experiments have come to the same conclusion.[6]

Nature of the Molecular Complex. For the indenyl system, the molecular interaction in the molecular complex [(C_9H_7)Fe$(CO)_2$R, phosphine] was interpreted in terms of an electron donor−acceptor mechanism, where the iron complex behaves as donor and phosphine as acceptor.[6] In this work, the Mulliken population analysis supports this idea and shows that the PH_3 behaves as an electron acceptor in the neutral molecular complex **3**. However, NPA analysis predicts that PH_3 remains almost neutral in **3**. To gain an insight into the nature of the molecular

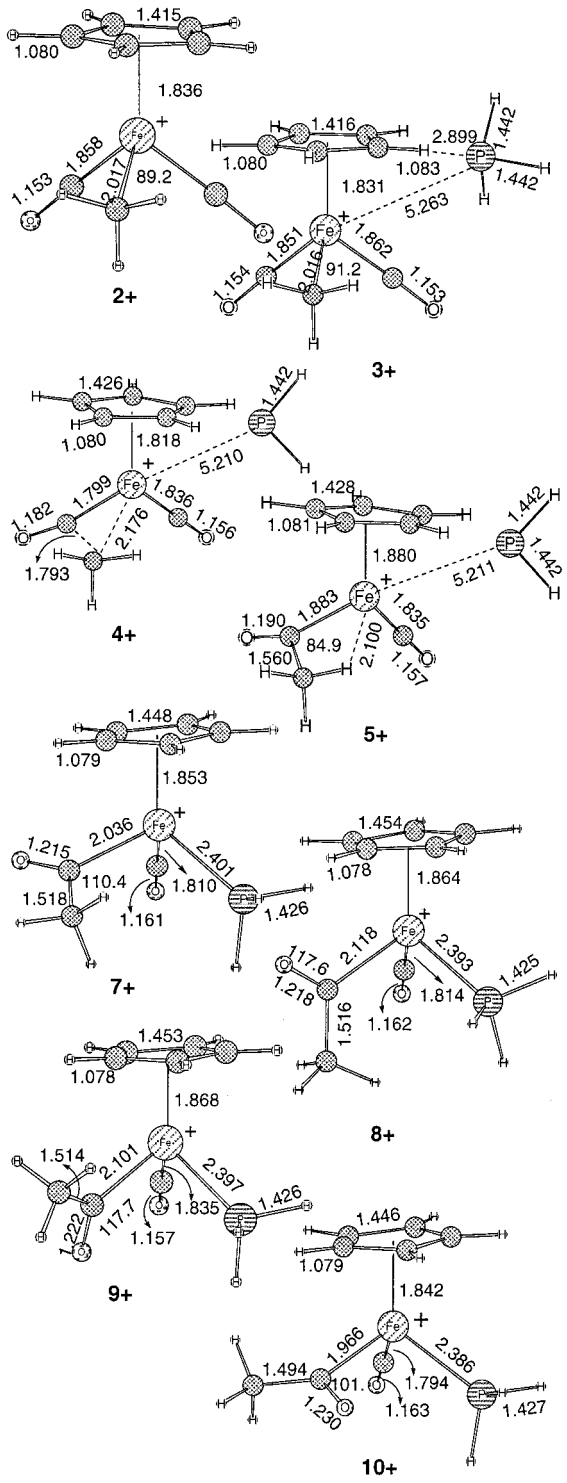

Figure 4. B3LYP-optimized geometries of the cation reactant **2**+, the molecular complex **3**+, transition states **4**+, **8**+, and **9**+, intermediates **5**+ and **7**+, and the final product **10**+ (only selected C−C and C−H bond lengths are given for the Cp ring).

complex, further donor−acceptor interaction analyses in the NBO basis were carried out.

Table 2 summarizes the interaction of the donor NBOs with the acceptor NBOs in a second-order perturbation estimate of the energy lowering. For the neutral molecular complex **3**, the interaction where PH_3 behaves as an acceptor and the iron complex as a donor is stronger than that where PH_3 behaves as a donor. In contrast to the case of **3**, PH_3 essentially behaves as a donor in the cation molecular complex **3**+. Note that the important NBO contributions to the donor−acceptor interaction

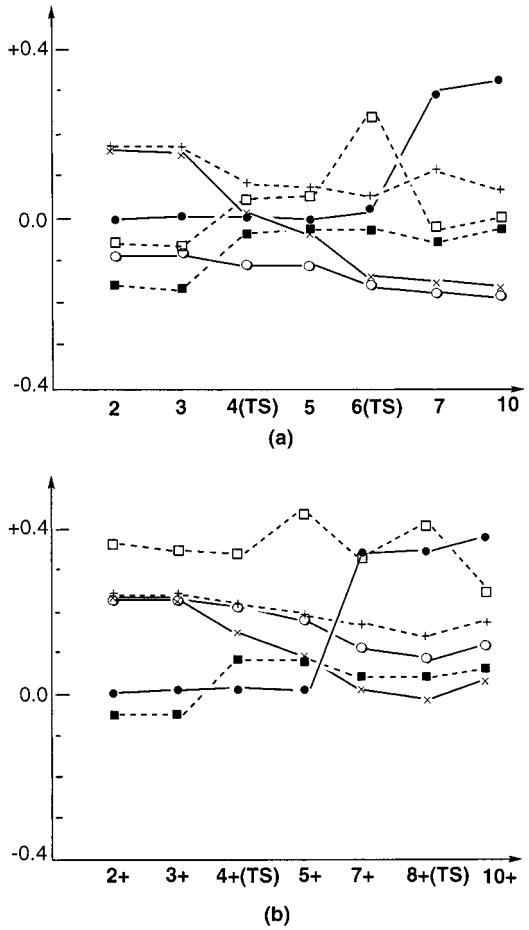

Figure 5. Net charges concentrated on subunits Fe, PH_3, CH_3, CO, and C_5H_5 ring along the reaction path obtained by natural population analysis: (×) CO (inactive); (+) CO (reactive); (○) C_5H_5;(□) Fe; (■) CH_3; ●: PH_3.

SCHEME 3

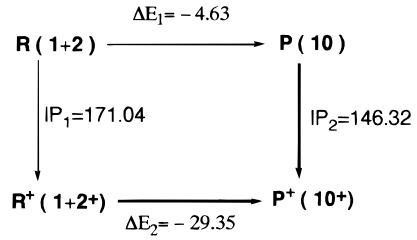

in the iron complex are antibonding orbitals of Fe−CO and C−H. The σ^*_{Fe-CO} NBOs are mainly composed of 3d/4s hybrid orbitals of Fe. The orientation of these NBOs in the iron complex, along with the electrostatic and van der Waals forces, governs the site and orientation of PH_3 in the optimized geometries.

Vibrational Properties. Table 3 reports vibrational frequencies of the carbonyl and the acyl group along the reaction path for both the neutral and the cation system. The DFT calculations are in reasonable agreement with the spectroscopic parameters of the neutral reactant **2** and the neutral product **10**. From the reactant to the product, the absorption position for the remaining carbonyl group shifts 42 cm^{-1} to lower frequency. A similar shift can be found for the cation system. This shift reflects the replacement of the strong π acceptor, CO, by a strong σ donor, PR_3. The strong bands of the terminal metal carbonyl and the acyl modes in the short-lived intermediate **5** appear at 1957 and 1772 cm^{-1}, respectively. Although these values are close to the

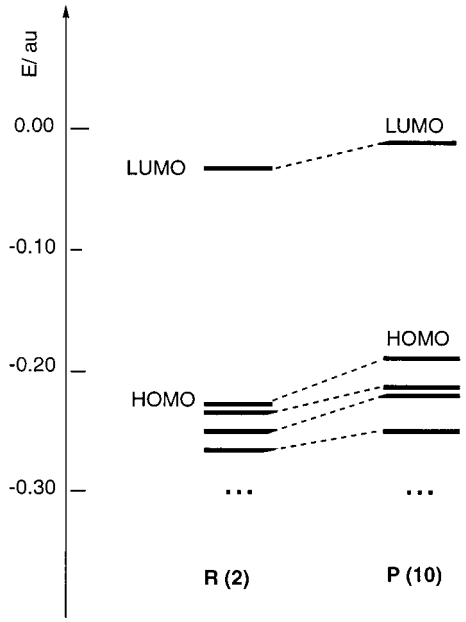

Figure 6. Energy levels of outer orbitals in the reactant **2** and the product **10**.

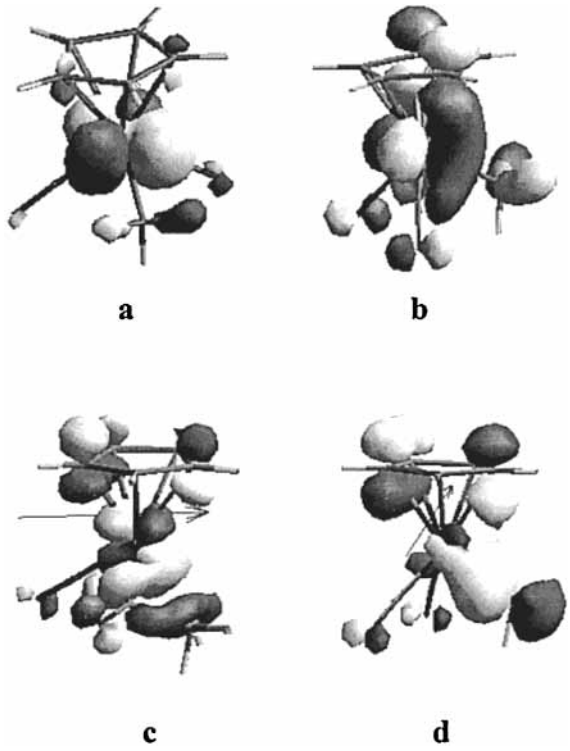

Figure 7. Spatial distributions of selected molecular orbitals (PH_3 frame in **5**+ and **3**+ are omitted): (a) the singly HOMO of **2**+; (b) the HOMO of **2**; (c) the singly HOMO of **5**+; (d) the MO corresponding to the Fe−CH_3 bond of **3**+.

experimental values of 1949 and ∼1610 cm^{-1} reported for the intermediate,[5] species **7** with two strong bands at 1957 and 1641 cm^{-1} is a much better match for the experimental values. Additional experimental studies will be necessary for the definitive assignment of the vibrational spectra for the observed intermediate. Compared to the neutral system, the corresponding bands in the cation system appear at higher frequency.

Stability of the η^2-Intermediate. The B3LYP/BS1-optimized geometries of the η^2-intermediates without the presence of phosphine are illustrated in Figure 8. The η^2-acyl intermediates, **5b** and **5b**+, are more stable than the η^2-methyl (agostic)

TABLE 2: Donor−Acceptor Interactions Estimated by the Second-Order Perturbation Theory in the NBO Basis

donor	acceptor	$\Sigma \Delta E_{ij}$[a]
	neutral **3**	
$Fe(CO)_2CH_3$	PH_3	8.36
(σ^*_{Fe-CO}/0.33637)[b]	(4p/0.00096)	
PH_3	Cp	0.98
(lone pair/1.99659)	(σ^*_{C-H}/0.01424)	
	cation **3**+	
$CpFe(CO)_2CH_3^+$	PH_3	0.47
(σ^*_{Fe-CO}/0.39666)	(σ^*_{P-H}/0.00297)	
PH_3 (lone pair)	Cp	3.44
(lone pair/1.98725)	(σ^*_{C-H}/0.02087)	

[a] Summation of the interaction ΔE_{ij} of donor NBO(i) with acceptor NBO(j) in kcal/mol. [b] NBO and occupancy of predominant contribution to the interaction and σ^*_{C-H} indicates the C−H bond in Cp ring close to PH_3.

TABLE 3: Vibrational Frequencies and Corresponding Intensities of the Carbonyl and the Acyl Group along the Reaction Path[a]

species	ν_{CO}	expt[b]	ν_{COR}	expt[b]
2	1999(649)	2014(7000)		
	1959(822)	1961(7000)		
3	1993(638)			
	1950(897)			
4(TS)	1960(794)		1826(634)	
5	1957(813)	1949	1772(597)	∼1610
6(TS)	1956(730)		1691(506)	
7	1957(764)	1949	1641(238)	∼1610
9	1939(717)		1635(245)	
10	1937(733)	1924(4100)	1620(246)	1612(∼400)
2+	2097(458)			
	2066(516)			
3+	2095(444)			
	2063(535)			
4+(TS)	2078(490)		1938(537)	
5+	2066(569)		1845(569)	
7+	2039(548)		1747(446)	
9+(TS)	2058(488)		1717(335)	
10+	2026(552)		1700(192)	

[a] Frequencies in cm^{-1} and IR intensities in parentheses in km/mol. [b] Values in parentheses indicate the absorbencies ϵ in M^{-1} cm^{-1}, taken from ref 5.

intermediates, **5a** and **5a**+, by 6.1 and 11.1 kcal/mol, respectively. In previous work on the migratory insertion in CpCO(NO)(CH_3), Niu and Hall,[16] observed a similar stability difference in η^2-intermediates of $CpCoN(O)CH_3$. They ascribed the stabilization of the η^2-nitrosyl intermediate to a strong Co−O−N three-center interaction, where the remnants of the in-plane π^* of NO behave as a π acceptor from Co. Presumably, similar interactions are responsible for stabilization of the η^2-acyl intermediates here.

To determine if these η^2-acyl intermediates are involved in the favored pathway for the migratory-insertion reaction, conversions from **5a** to **5b** and from **5a**+ to **5b**+ were investigated. The barriers of formation of **5b** from **5a** by rotation are 12.8 (**TSa**) for clockwise and 14.7 kcal/mol (**TSb**) for counterclockwise, respectively. A pure swinging transition state was found to have a barrier of 14.7 kcal/mol. Despite careful selection of different initial guesses for the rotating and swinging transition state searches for **5a**+ to **5b**+, serious spin contamination could not be avoided in the unrestricted open-shell B3LYP calculation. Spin contamination was not a problem for the other cation species **2**+ to **10**+, including **5a**+ and **5b**+. A spin contaminated swinging transition state ($S^2 = 1.5$) is 3.2 kcal/mol above **5a**+. The single-point calculation by the unrestricted open-shell B3LYP ($S^2 = 0.97$) with initial MOs

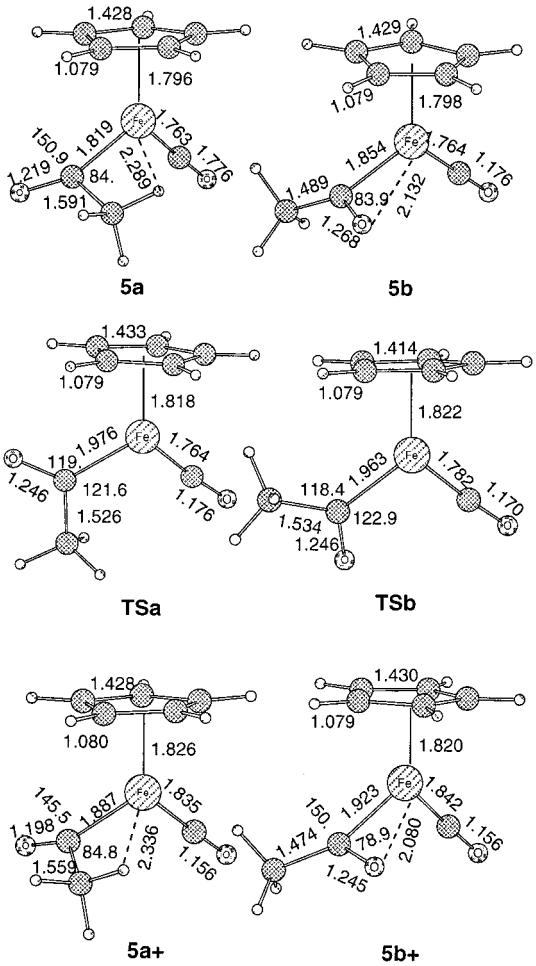

Figure 8. B3LYP-optimized geometries of the η^2-intermediates **5a**, **5a**+, **5b**, **5b**+, and the transition states **TSa** and **TSb**.

from a restricted open-shell B3LYP calculation predicted the swinging transition state to be higher in energy than the **5a**+ by 8.7 kcal/mol. Another approximate swinging-rotating transition state ($S^2 = 1.7$) is less stable by 13 kcal/mol than the **5a**+. Although serious spin contamination makes these barriers less reliable, one can safely say that a barrier exists for the formation of **5b**+ from **5a**+. It is only in this minor side reaction that evidence for low-lying, high-spin states was observed.

Note that those barriers for the PH_3 association to **5** and **5**+ are 4.8 and ~0 kcal/mol along the favored reaction paths (Figures 1 and 3), respectively. Therefore, one can reasonably conclude that these η^2-acyl intermediates are not critical components in either of these migratory-insertion reactions.

Conclusion

Theoretical investigations of the CO insertion reactions for the neutral system and the oxidatively promoted process have been presented. DFT calculations show that the intramolecular methyl migration is the rate-determining step for both reactions. The calculated activation energies for the rate-determining step are 17.8 and 7.5 kcal/mol, respectively, for the neutral reaction and the cation reaction at the DFT level with the larger basis set. This work supports the experimental conclusion that the neutral thermally driven migratory insertion reaction is irreversible at 80 °C but reversible at 100 °C, and that the oxidatively promotion insertion is exceedingly rapid even at −40 °C.[9a] The difference of the electronic structure between the neutral reactant and the cation reactant accounts for their different reactivities. In the cation reaction, the unpaired electron on Fe provides a mechanism for making the methyl migration more radical in character, while the neutral migration has more methyl anion $:CH_3^-$ character. The calculations do not support a different mechanism for the cation reaction nor do they support ring slippage as a possibility. The DFT calculations also reproduce the observed geometries and vibrational frequencies. Donor−acceptor interaction analyses support the idea that the phosphine behaves as weak acceptor in the neutral molecular complex, while in the cation molecular complex the phosphine is a donor. In both reactions added phosphine plays a minor role until the migratory insertion phase is complete.

Acknowledgment. We gratefully acknowledge the National Science Foundation (Grant No. CHE 9800184) and The Welch Foundation (Grant No. A-648) for financial support of this work.

References and Notes

(1) Collman, J. A.; Hegedus, L. S.; Norton, J. R.; Finke, R. G. *Principles and Applications of Organotransition Metal Chemistry*; University Science Books: Mill Valley, CA, 1987.

(2) (a) Biller, J. P.; Wojcicki, A. *Inorg. Chem.* **1966**, *5*, 889. (b) Butler, I. S.; Basolo, F.; Pearson, R. G. *Inorg. Chem.* **1967**, *6*, 2074.

(3) Green, M.; Westlake, D. J. *J. Chem. Soc. A* **1971**, 367.

(4) Wax, M. J.; Bergman, R. G. *J. Am. Chem. Soc.* **1981**, *103*, 7028.

(5) (a) Belt, S. T.; Ryba, D. W.; Ford, P. C. *J. Am. Chem. Soc.* **1991**, *113*, 9524. (b) McFarlane, K. L.; Lee, B.; Fu, W.; van Eldik, R.; Ford, P. C. *Organometallics* **1998**, *17*, 1826. (c) Rerek, M. E.; Ji, L.-N.; Basolo, F. *J. Chem. Soc., Chem. Commun.* **1983**, 1208. (d) Belmont, J. A.; Wrighton, M. S. *Organometallics* **1986**, *5*, 1421.

(6) (a) Monti, D.; Bassetti, M. *J. Am. Chem. Soc.* **1993**, *115*, 4658. (b) Bassetti, M.; Mannina, L.; Monti, D. *Organometallics* **1994**, *13*, 3293.

(7) O'Connor, J. M.; Casey, C. P. *Chem. Rev.* **1987**, *87*, 307.

(8) Schonberg, P. R.; Paine, R. T.; Campana, C. F.; Duesler, E. N. *Organometallics* **1982**, *1*, 799.

(9) (a) Colletti, S. L.; Halterman, R. L. *Organometallics* **1992**, *11*, 980. (b) Therien, M. J.; Trogler, W. C. *J. Am. Chem. Soc.* **1987**, *109*, 5127. (c) Magnuson, R. H.; Meirowitz, R.; Zulu, S.; Giering, W. P. *J. Am. Chem. Soc.* **1982**, *104*, 5790. (d) Magnuson, R. H.; Meirowitz, R.; Zulu, S.; Giering, W. P. *Organometallics* **1983**, *2*, 460. (e) Miholova, D.; Vlcek, A. A. *J. Organomet. Chem.* **1982**, *240*, 413.

(10) (a) Berke, H.; Hoffmann, R. *J. Am. Chem. Soc.* **1978**, *100*, 7224. (b) Hofmann, P.; Stauffert, P.; Tatsumi, K.; Nakamura, A.; Hoffmann, R. *Organometallics* **1985**, *4*, 404. (c) Hofmann, P.; Stauffert, P.; Tatsumi, K.; Nakamura, A.; Hoffmann, R. *J. Am. Chem. Soc.* **1985**, *107*, 4440.

(11) Curtis, M. D.; Shiu, K.-B.; Butler, W. M. *J. Am. Chem. Soc.* **1986**, *108*, 1550.

(12) Ziegler, T.; Versluis, L.; Tschinke, V. *J. Am. Chem. Soc.* **1986**, *108*, 612.

(13) (a) Axe, F. U.; Marynick, D. S. *Organometallics* **1987**, *6*, 572. (b) Axe, F. U.; Marynick, D. S. *J. Am. Chem. Soc.* **1988**, *110*, 3728.

(14) (a) Sakaki, S.; Kitaura, K.; Morokuma, K.; Ohkabo, K. *J. Am. Chem. Soc.* **1983**, *105*, 2280. (b) Koga, N.; Morokuma, K. *J. Am. Chem. Soc.* **1985**, *107*, 7230.

(15) Rappé, A. K. *J. Am. Chem. Soc.* **1987**, *109*, 5605.

(16) Niu, S.-Q.; Hall, M. B. *J. Phys. Chem. A* **1997**, *101*, 1360; *J. Am. Chem. Soc.* **1997**, *119*, 3077.

(17) Derecskei-Kovacs, A.; Marynick, S. D. *J. Am. Chem. Soc.* **2000**, *122*, 2078.

(18) Niu, S.-Q.; Hall, M. B. *Chem. Rev.* **2000**, *100*, 353.

(19) Becke, A. D. *J. Chem. Phys.* **1993**, *98*, 5648.

(20) Lee, C.; Yang, W.; Parr, R. G. *Phy. Rev.* **1988**, *B37*, 785.

(21) Frisch, M. J.; Trucks, G. W.; Schlegel, H. B.; Gill, P. M. W.; Johnson, B. G.; Robb, M. A.; Cheeseman, J. R.; Keith, T.; Petersson, G. A.; Montgomery, J. A.; Raghavachari, K.; Al-Laham, M. A.; Zakrzewski, V. G.; Ortiz, J. V.; Foresman, J. B.; Peng, C. Y.; Ayala, P. Y.; Chen, W.; Wong, M. W.; Andres, J. L.; Replogle, E. S.; Gomperts, R.; Martin, R. L.; Fox, D. J.; Binkley, J. S.; Defrees, D. J.; Baker, J.; Stewart, J. P.; Head-Gordon, M.; Gonzalez, C.; Pople, J. A. *Gaussian 94*, Revision B.3; Gaussian Inc.: Pittsburgh, PA, 1994.

(22) (a) Weinhold, F.; Carpenter, J. E. *The Structure of Small Molecules and Ions*; Plenum: New York, 1988; p 227. (b) Reed, A. E.; Curtiss, L. A. Weinhold, F. *Chem. Rev.* **1988**, *88*, 899. (c) Reed, A. E.; Weinstock, R. B.; Weinhold, F. *J. Chem. Chem.* **1985**, *83*, 735. (d) Reed, A. E.; Weinhold, F. *J. Chem. Phys.* **1983**, 1736. (e) Reed, A. E.; Weinhold, F. *J. Chem. Phys.* **1983**, *78*, 4066. (f) Foster, J. P.; Weinhold, F. *J. Am. Chem. Soc.* **1980**,

102, 7211. (g) Carpenter, J. E. Ph.D. Thesis, University of Wisconsin, 1987. (h) Carpenter, J. E.; Weinhold, F. *J. Mol. Struct.* (*THEOCHEM*) **1988**, *169*, 41.

(23) Hay, P. J.; Wadt, W. R. *J. Chem. Phys.* **1985**, *82*, 299.

(24) Couty, M.; Hall, M. B. *J. Comput. Chem.* **1996**, *17*, 1359.

(25) Ditchfield, R.; Hehre, W. J.; Pople, J. A. *J. Chem. Phys.* **1971**, *54*, 724.

(26) Hehre, W. J.; Ditchfield, R.; Pople, J. A. *J. Chem. Phys.* **1972**, *56*, 2257.

(27) Hariharan, P. C.; Pople, J. A. *Mol. Phys.* **1974**, *27*, 209.

(28) Gordon, M. S. *Chem. Phys. Lett.* **1980**, *76*, 163.

(29) Hariharan, P. C.; Pople, J. A. *Theo. Chim. Acta.* **1973**, *28*, 213.

(30) (a) Höllwarth, A.; Böhme, M.; Dapprich, S.; Ehlers, A. W.; Gobbi, A.; Jonas, V.; Köhler, K. F.; Stegmann, R.; Veldkamp, A.; Frenking, G. *Chem. Phys. Lett.* **1993**, *208*, 111. (b) Boys, S. F.; Bernardi, F. *Mol. Phys.* **1970**, *19*, 553.

(31) (a) Kuhlmann, E. K.; Alexander, J. J. *J. Coord. Chem. Rev.* **1980**, *33*, 195. (b) Kurfee, L. D.; Rothwell, I. P. *Chem. Rev.* **1988**, *88*, 1059.

(32) Ambrosi, L.; Bassetti, M.; Buttiglieri, P.; Mannina, L.; Monti, D.; Bocelli, G. *J. Organomet. Chem.* **1993**, *455*, 167.

(33) (a) Churchill, M. R.; Wormadld, J. *Inorg. Chem.* **1969**, *8*, 1936. (b) Davis, R. E. *Chem. Commun.* **1969**, 1218.